ACS OMEGA

http://pubs.acs.org/journal/acsodf

Article

Novel 5-(Arylideneamino)-1*H*-Benzo[*d*]imidazole-2-thiols as Potent Anti-Diabetic Agents: Synthesis, In Vitro α-Glucosidase Inhibition, and Molecular Docking Studies

Sardar Ali,* Mumtaz Ali,* Ajmal Khan, Saeed Ullah, Muhammad Waqas, Ahmed Al-Harrasi, Abdul Latif, Manzoor Ahmad, and Muhammad Saadiq

Cite This: *ACS Omega* 2022, 7, 43468−43479

Read Online

ACCESS | Metrics & More | Article Recommendations | Supporting Information

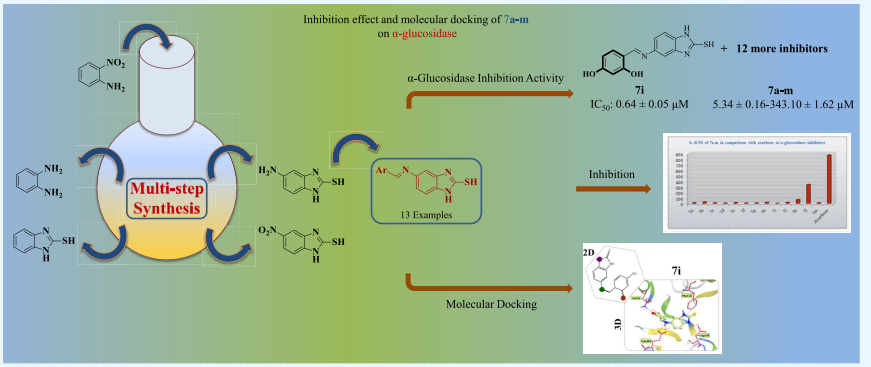

ABSTRACT: A novel series of multifunctional benzimidazoles has been reported as potent inhibitors of α-glucosidase. The procedure relies on the synthesis of 5-amino-1*H*-benzo[*d*]imidazole-2-thiol **5** via the multistep reaction through 2-nitroaniline **1**, benzene-1,2-diamine **2**, 1*H*-benzo[*d*]imidazole-2-thiol **3**, and 5-nitro-1*H*-benzo[*d*]imidazole-2-thiol **4**. Further treatment of **5** with aromatic aldehydes **6a−m** provided access to the target 5-(arylideneamino)-1*H*-benzo[*d*]imidazole-2-thiols **7a−m**. The results of the bioactivity assessment revealed all the compounds as excellent inhibitors of the enzyme (IC_{50} range: 0.64 ± 0.05 μM to 343.10 ± 1.62 μM) than **acarbose** (873.34 ± 1.21). Among them, **7i** was the most active inhibitor (IC_{50}: 0.64 ± 0.05 μM) followed by **7d** (IC_{50}: 5.34 ± 0.16 μM), **7f** (IC_{50}: 6.46 ± 0.30 μM), **7g** (IC_{50}: 8.62 ± 0.19 μM), **7c** (IC_{50}: 9.84 ± 0.08 μM), **7m** (IC_{50}: 11.09 ± 0.79 μM), **7a** (IC_{50}: 11.84 ± 0.26 μM), **7e** (IC_{50}: 16.38 ± 0.53 μM), **7j** (IC_{50}: 18.65 ± 0.74 μM), **7h** (IC_{50}: 20.73 ± 0.59 μM), **7b** (IC_{50}: 27.26 ± 0.30 μM), **7k** (70.28 ± 1.52 μM) and finally **7l** (IC_{50}: 343.10 ± 1.62 μM). Molecular docking revealed important interactions with the enzyme, thereby supporting the experimental findings.

INTRODUCTION

Type 2 diabetes mellitus (**T2DM**) is a chronic metabolic disorder, characterized by elevated blood glucose levels. It is one of the major threats to human health in the 21st century disrupting the metabolism of carbohydrates, proteins, and lipids.[1] Obesity, physical inertness, and oxidative stress are the major factors causing **T2DM**,[2] which can lead to serious complications such cardiovascular diseases, retinopathy, neuropathy, nephropathy, and so forth.[3] The International Diabetes Federation (IDF) has reported 425 million patients with diabetes globally in 2017, which is estimated to increase to 629 million by 2045.[4] Two enzymes, α-amylase and α-glucosidase, play key roles in carbohydrate metabolism, thereby increasing blood glucose (hyperglycemia). The inhibition of these enzymes has found an effective way of managing **T2DM.**[5]

Pakistan is a South Asian country with a population of 207.68 million people (Pakistan Bureau of Statistics, 2017). The national diabetes survey of Pakistan in 1999 reported the prevalence of diabetes as 11%;[6] however, this number has alarmingly increased in the 21st century. The IDF Atlas 2017 has ranked Pakistan at 10 of 221 countries of the world having 7.5 million cases of diabetes aged 20−79 years,[7] while in its recent survey (IDF Atlas 9th Edition 2019), the prevalence of diabetes in Pakistan has reached 17.1% (19 million adults with diabetes), which is 148% higher than the previously reported figures.[8] This alarming situation of growing diabetes crisis needs immense attention.

Received: June 20, 2022
Accepted: November 7, 2022
Published: November 23, 2022

Scheme 1. Synthetic Route Leading to the Target Compounds 7a−m

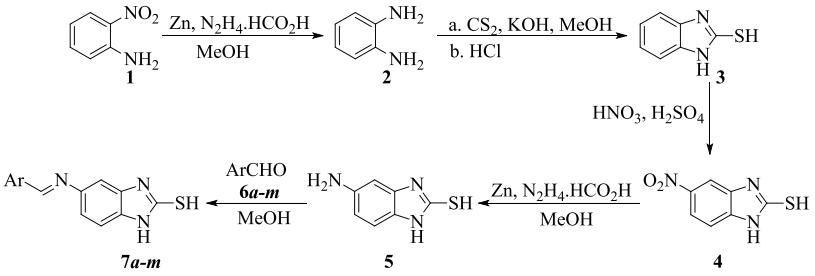

Table 1. In Vitro α-Glucosidase Inhibition Activity of the Target Compounds 7a−m

sample	percent inhibition (0.5 mM)	IC_{50} ± μM (SEM)
7a	95.68	11.84 ± 0.26
7b	93.25	27.26 ± 0.30
7c	95.74	9.84 ± 0.08
7d	96.61	5.34 ± 0.16
7e	91.35	16.38 ± 0.53
7f	95.00	6.46 ± 0.30
7g	94.86	8.62 ± 0.19
7h	91.70	20.73 ± 0.59
7i	95.41	0.64 ± 0.05
7j	94.73	18.65 ± 0.74
7k	87.64	70.28 ± 1.52
7l	83.20	343.10 ± 1.62
7m	94.00	11.09 ± 0.79
acarbose	58.49	873.34 ± 1.21

Benzimidazole is a privileged structure in organic and medicinal chemistry as is evident from its different medicinal candidates such as omeprazole, pantoprazole (proton pump inhibitors), triclabendazole, thiabendazole, albendazole, mebendazole (anthelmintic), benomyl, carbendazim, fuberidazole (fungicide), candesertan, telmisartan (anti-hypertensive), astemizole (antihistamine), bendamustine (anti-cancer), afobazole (anxiolytic), and so forth.[9] New synthetic analogues of benzimidazole have been continuously reported to have a broad spectrum of activities. Our research group has previously reported benzimidazole-based antioxidants (IC_{50}: 131.50 ± 12.39; IC_{50}: 167.4 ± 7.4), α-glucosidase (IC_{50}: 352 μg/mL), cholinesterase (IC_{50}: 121.2 μM and 38.3 μM), and carbonic anhydrase inhibitors (IC_{50}: 13.3 ± 1.25 μM).[10,11]

In search of exploring new benzimidazole-based medicinal candidates, the present study was aimed at designing, synthesis, and bioactivity assessment of novel benzimidazole derivatives.

RESULTS AND DISCUSSION

This work is based on a multistep reaction procedure. The target compounds **7a−m** were accomplished using methods, as outlined in Scheme 1. In the first step, 2-nitroaniline **1** was reduced to benzene-1, 2-diamine **2**. Then, it was cyclized to 1*H*-benzo[*d*]imidazole-2-thiol **3** through CS_2. The obtained product **3** was oxidized to 5-nitro-1*H*-benzo[*d*]imidazole-2-thiol **4** and then reduced to 5-amino-1*H*-benzo[*d*]imidazole-2-thiol **5**. Finally, the reaction of **5** with different aromatic aldehydes **6a−m** yielded the target compounds **7a−m**. The synthesis of all the compounds was monitored by their thin-layer chromatography (TLC) analysis in *n*-hexane: ethyl acetate/chloroform systems under UV. The structures of all the compounds were confirmed with the help of ESI-HRMS, ^{1}HNMR, and ^{13}CNMR spectroscopy.

The target compounds **7a−m** in their ^{1}H NMR spectra displayed protons of the thiol and *sec*-amine (−SH, −NH−) at δ 12.688−12.479, imine protons (−N=CH−) at δ 8.965−8.396 ppm, aromatic protons at δ 8.353−6.280 ppm, as well as other substituents such as OH, CH_3, OCH_3, and −N-$(CH_2CH_3)_2$ etc. at various chemical shift values. The ^{13}C NMR spectra showed the carbon skeleton of the compounds highlighting the carbons of the aromatic rings, imine and alkyl at δ 169.12−12.47 ppm. The ESI-HRMS displayed the molecular ion peaks $(M + H)^+$ of the compounds and various fragment ions. After structural confirmation, they were evaluated for α-glucosidase inhibition potential which is further discussed in the biological activity section.

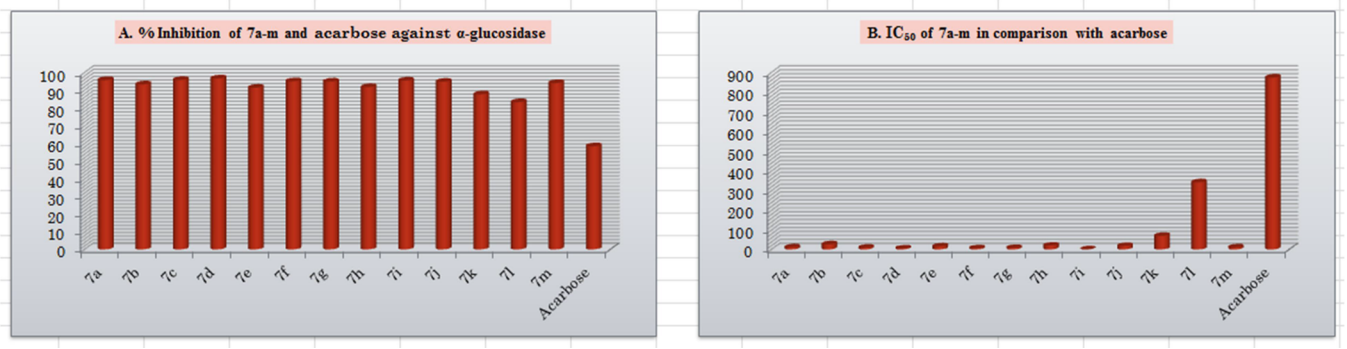

Figure 1. (A) % Inhibition of **7a−m** against α-glucosidase in comparison with acarbose. (B) IC_{50} of **7a−m** against α-glucosidase in comparison with acarbose.

https://doi.org/10.1021/acsomega.2c03854
ACS Omega 2022, 7, 43468−43479

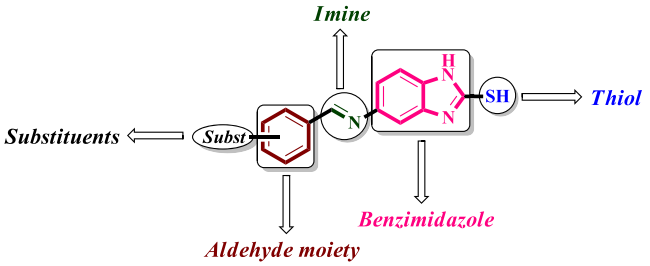

Figure 2. Various functional groups in the general structure of the target compounds **7a−m**.

BIOLOGICAL EVALUATION

***α*-Glucosidase Inhibitory Activity of the Target Compounds 7a−m.** The in vitro *α*-glucosidase inhibition potential of the target compounds **7a−m** was evaluated using **acarbose** as a standard antidiabetic drug.[12] As shown in Table 1, all the tested compounds displayed the highest inhibition of the enzyme than acarbose (IC_{50}: 873.34 ± 1.21 *μ*M), where **7i** was the most active inhibitor (IC_{50}: 0.64 ± 0.05 *μ*M) followed by **7d** (IC_{50}: 5.34 ± 0.16 *μ*M), **7f** (IC_{50}: 6.46 ± 0.30 *μ*M), **7g** (IC_{50}: 8.62 ± 0.19 *μ*M), **7c** (IC_{50}: 9.84 ± 0.08 *μ*M), **7m** (IC_{50}: 11.09 ± 0.79 *μ*M), **7a** (IC_{50}: 11.84 ± 0.26 *μ*M), **7e** (IC_{50}: 16.38 ± 0.53 *μ*M), **7j** (IC_{50}: 18.65 ± 0.74 *μ*M), **7h** (IC_{50}: 20.73 ± 0.59 *μ*M), **7b** (IC_{50}: 27.26 ± 0.30 *μ*M), **7k** (70.28 ± 1.52 *μ*M), and finally **7l** (IC_{50}: 343.10 ± 1.62 *μ*M) which was the last inhibitor in the series.

The comparative % inhibition of *α*-glucosidase and the IC_{50} values of the target compounds with reference to acarbose are provided in Figure 1a,b. It is clear from the two graphs that the inhibition potential of target compounds **7a−m** is much better than that of the reference drug.

Structure Activity Relationship. The target compounds **7a−m** are multifunctional benzimidazoles, as shown in Figures 2 and 3. Figure 2 represents their basic skeleton where

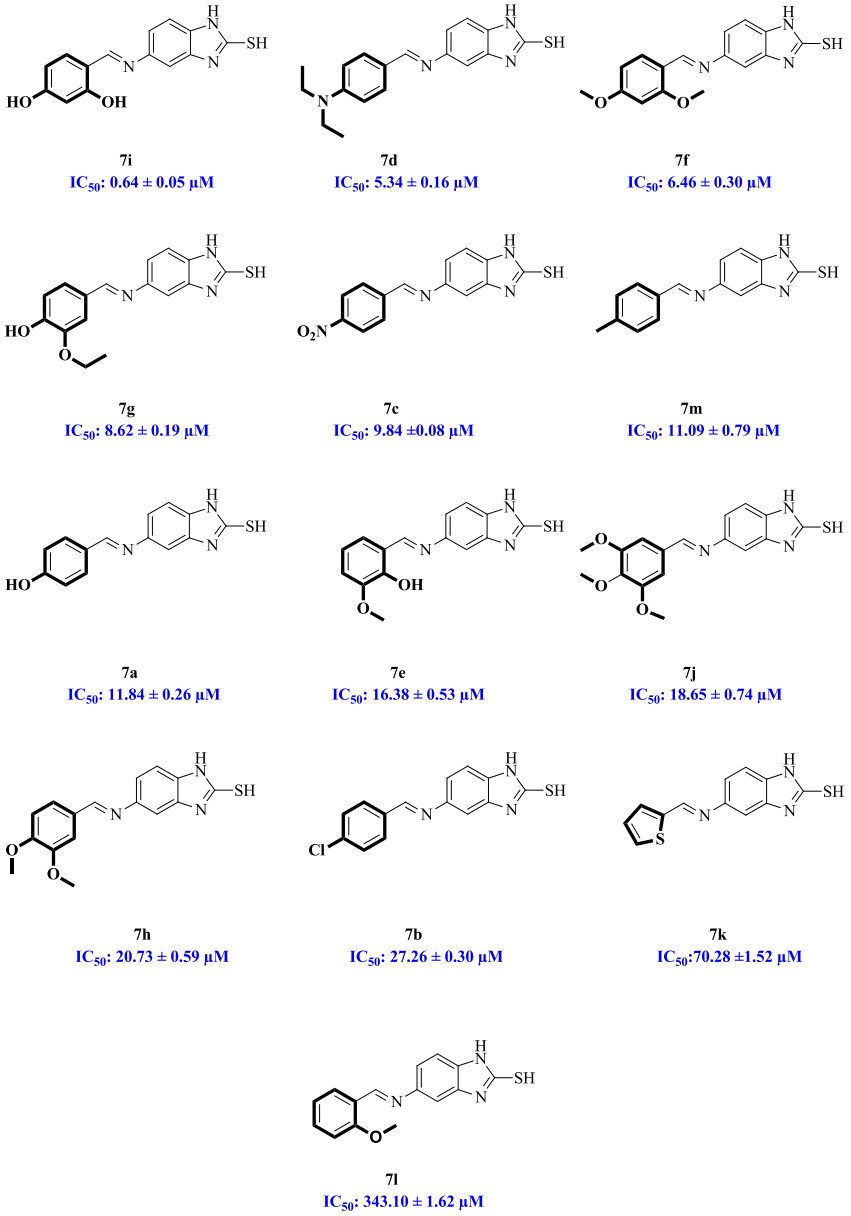

Figure 3. Structures of the 13 inhibitors **7a−m** of *α*-glucosidase with their IC_{50} values.

https://doi.org/10.1021/acsomega.2c03854
ACS Omega 2022, 7, 43468−43479

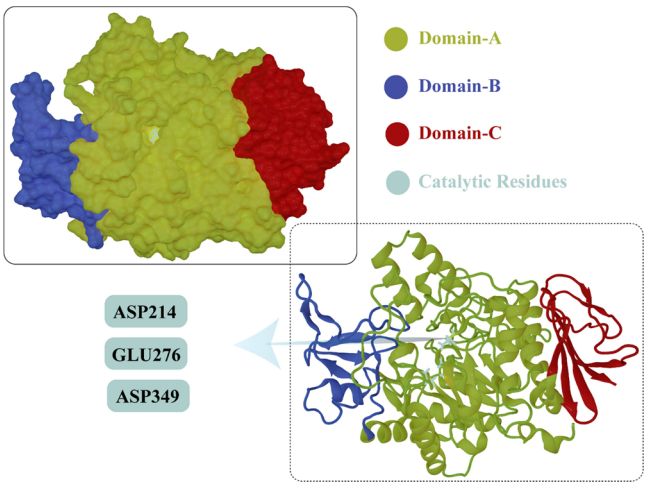

Figure 4. 3D structure of α-glucosidase (surface and cartoon representation defining the catalytic residues in cyan). Yellow represents domain **A** (amino acids 1−113 and 190−512), blue represents domain **B** (amino acids 114−189), and red represents domain **C** (amino acids 513−589).

benzimidazole bears a thiol group at C-2 and an imine group at C-5 to which various aromatic substituents are bonded.

These compounds bear differences in the substituents at the benzylidene ring except **7k** where a thiophene ring bonds the imine carbon. **7i** and **7f** are 2,4-disubstituted while **7a**, **7b**, **7c**, **7d**, and **7m** are 4-substituted benzylidene analogues. Furthermore, **7g** and **7h** are 3,4-disubstituted, **7e** is 2-3-disubstituted, **7j** is 3,4,5-trisubstituted while **7l** is 2-substituted analogue. Lastly, **7k** is thiophen-2-ylmethylene analogue as shown in Figure 3. All the substituents present at the 2nd, 3rd, 4th, and 5th position of the benzylidene ring as well as the heterocyclic moiety have greatly enhanced the inhibition potential of the compounds. Overall, the 13 novel compounds evaluated against α-glucosidase inhibited the enzyme more than the standard inhibitor **acarbose** (IC_{50}: 873.34 ± 1.21 μM). All these compounds demand further investigation which may help in drug development against type 2 diabetes mellitus.

MOLECULAR DOCKING STUDIES

Methodology. To explore the interaction of the target compounds **7a−m** with the enzyme, a homology model of *S. cerevisiae* α-glucosidase (ID AF-P38158-F1) was downloaded from the AlphaFold Protein Structure Database server (https://alphafold.ebi.ac.uk/).[13] Ramachandran plot was generated to further validate the quality of the model (https://zlab.umassmed.edu/bu/rama/).[14] The allowed regions and disallowed residues were identified. Furthermore, the ProSA-web server was used to compute the stereochemical properties of the enzyme by comparing the model with the reported crystal structure.[15] Employing molecular mechanics, the missing hydrogens in the model were added using molecular operating environment (MOE-2020.0109)[16] and the partial charges were calculated using the tethered energy minimization implemented in MOE. The enzyme geometry was optimized using the autocorrect protocol of MOE and the bad contacts were removed. The low energy conformations of the enzyme was determined using the AMBER14:ETH force field.[17]

Three-Dimensional Structure of α-Glucosidase. The three-dimensional (3D) structure of the α-glucosidase is presented in Figure 4. The active site and catalytic residues of *S. cerevisiae* (PDB ID 3A47) and α-glucosidase (ASP214, GLU276, ASP349) are conserved for substrate attachment.[18] The three domains (**A**, **B**, **C**) of the enzyme are reported in different colors (yellow, blue, red) representing the amino acids.

Model Validation. To learn about the general structure of the model, the homology model of the enzyme must be validated. The Ramachandran plot demonstrates good stereo-

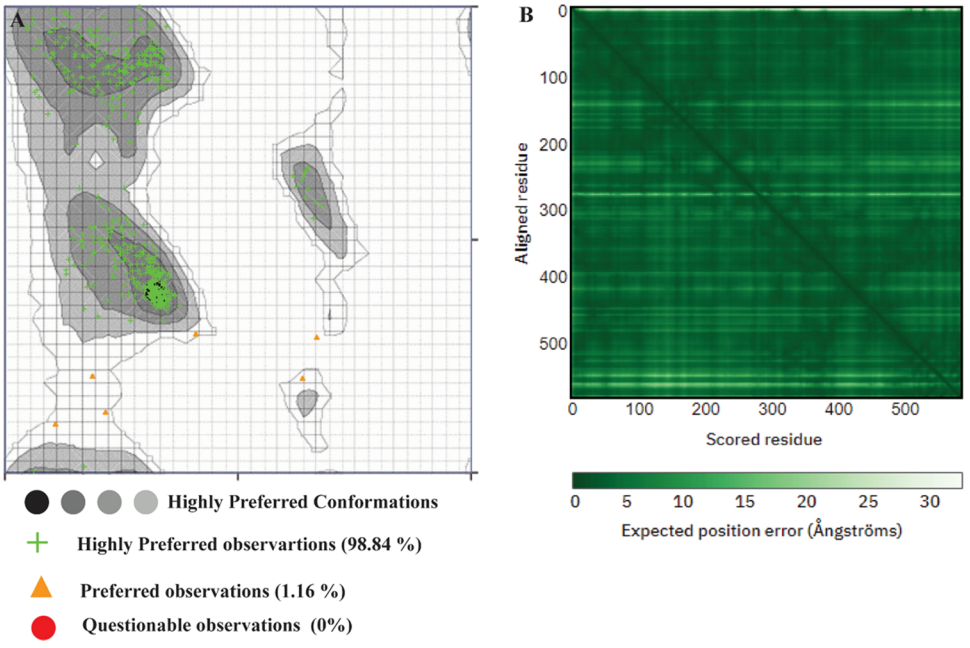

Figure 5. Structure evaluation of the 3D model of α-glucosidase by (A) Ramachandran plot analysis and (B) Error value of AlphaFold Protein Structure prediction database. Green color indicates the highly favorable regions of the enzyme, while orange color indicates the preferable regions. The prominent green color indicates zero error in the 90% region of the model.

https://doi.org/10.1021/acsomega.2c03854
ACS Omega 2022, 7, 43468−43479

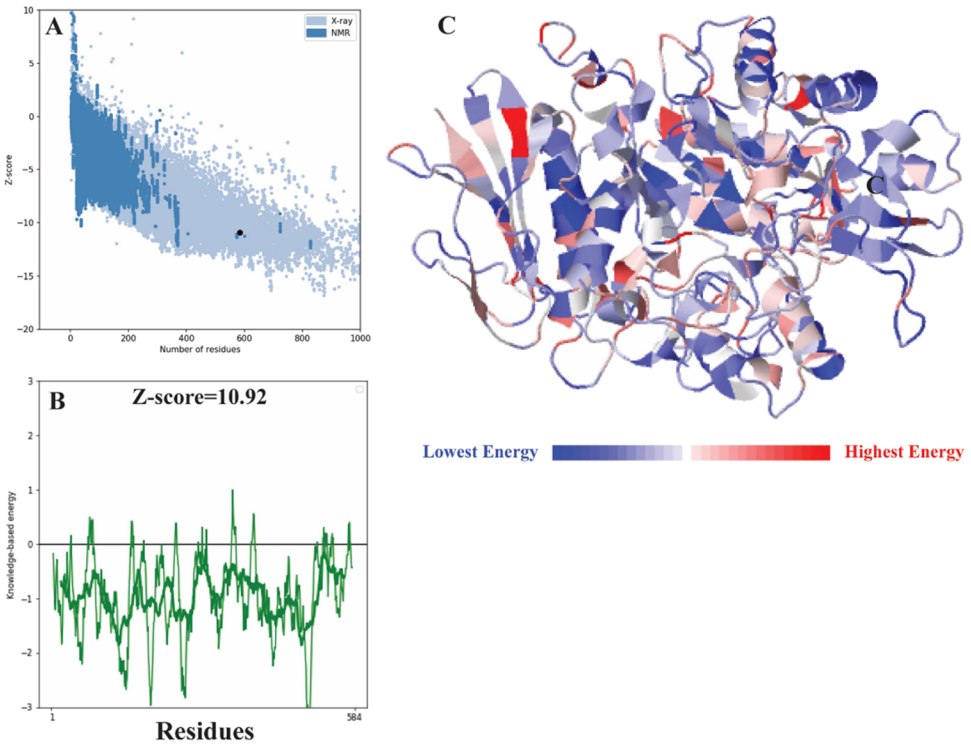

Figure 6. Overall quality of the α-glucosidase model from the ProSA-web server; (A) comparison with the crystal structures of the enzymes reported having the same size, (B) energy levels of the overall model residues, and (C) cartoon representation of the model with different energy level regions.

chemical characteristics of the model. The model's residues were in the favorable zone (98.84%), the allowed region was 1.16%, and there was no disallowed area in the 3D model of the enzyme. The AlphaFold Protein Structure alignment with the template expected error was zero in 90% of the model residues. The deviation from the template was calculated in angstrom (Å) (Figure 5).

The overall structural quality of α-glucosidase is depicted in Figure 6, revealing that the model was inside the acceptable quality zone. The small variations were at a positive energy state (enzyme's unstable areas), but the overall model was in a negative energy window (enzyme's overall excellent quality). The current model showed that the X-ray structure zone had the same amino acid size, offering excellent quality of the model. The high and low energy areas were highlighted in blue and red, respectively. The entire model was registered in a lower energy state, defining the enzyme structure's stability.

Docking Studies on α-Glucosidase. The docking protocols were validated by transferring the substrate molecule (isomaltose) from PDB ID 3AXH (*S. cerevisiae* isomaltase) because of high structural similarity and conserved catalytic residues (Asp214, Glu276, and Asp349) with the *S. cerevisiae* α-glucosidase. The conserved catalytic residues triad for substrate catalysis, where Asp349 maintained the transition state of the substrate molecule while Glu276 and Asp214 acted as nucleophile and proton donors, respectively. The lining of the active site residues includes Arg212, Glu276, Asp214, Tyr71, His348, Asp349, Arg439, Asp68, and Phe177 that form multiple hydrophilic and hydrophobic interactions with the substrate molecule (Figure 7). Redocking was performed, and the reported RMSD between the reported and redocked substrate is 0.729 Å, which appears to be an acceptable range. To explore the selected compound interactions at the atomic level, their stability and the best fit in the active pocket of the α-glucosidase protein molecular docking study was performed using MOE. The target compounds **7a−m** were docked in the active pocket residues of the 3D structure of the α-glucosidase, and the docking contacts were examined. All the compounds demonstrated excellent interactions with the active pocket residues. The important active site residues (catalytic residues) involved in the interaction with the compounds were ASP214, GLU276, and ASP349. Similarly, other residues in the surrounding were GLU276, GLU304, and GLY217 which have occupied the 1st, 2nd, and 3rd positions, respectively, in the interaction population (Figure 8).

The 3D interactions of the target compounds **7a−m** in the active pocket of the α-glucosidase along with their two-dimensional images are presented in Figure 9 which highlights the various parts of each compound involved with the residues.

Docking Score, Binding Energy, and Affinity. The binding energy and affinity were determined using MOE's implicit solvent technique generalized Born/volume integral (GB/VI). The generalized Born interaction is nonbonded interaction energy between an enzyme and the inhibitor.

The target compounds **7a−m** showed good binding energy, affinity, and docking score with slight variations (Table 2). The highest binding energy and affinity were reported for **7i** as −69.65 kcal/mol and −10.54 kcal/mol, for **7f** as −63.36 kcal/mol and −10.09 kcal/mol, and for **7d** as −57.02 kcal/mol and affinity −9.06 kcal/mol, respectively. On the other hand, **7j** displayed the highest docking score (−7.34 kcal/mol) and has formed hydrogen bond interactions with Asp68, His111, Gln181, and Asp214 while **7c**, **7e**, **7f**, **7g**, **7h**, **7i**, and **7m** displayed the 2nd highest docking (−6.1 to −6.5 kcal/mol) followed by **7a**, **7b**, **7d**, and **7k** (−5.7 to −5.9 kcal/mol), making good interactions with the active pocket of the enzyme.

https://doi.org/10.1021/acsomega.2c03854
ACS Omega 2022, 7, 43468−43479

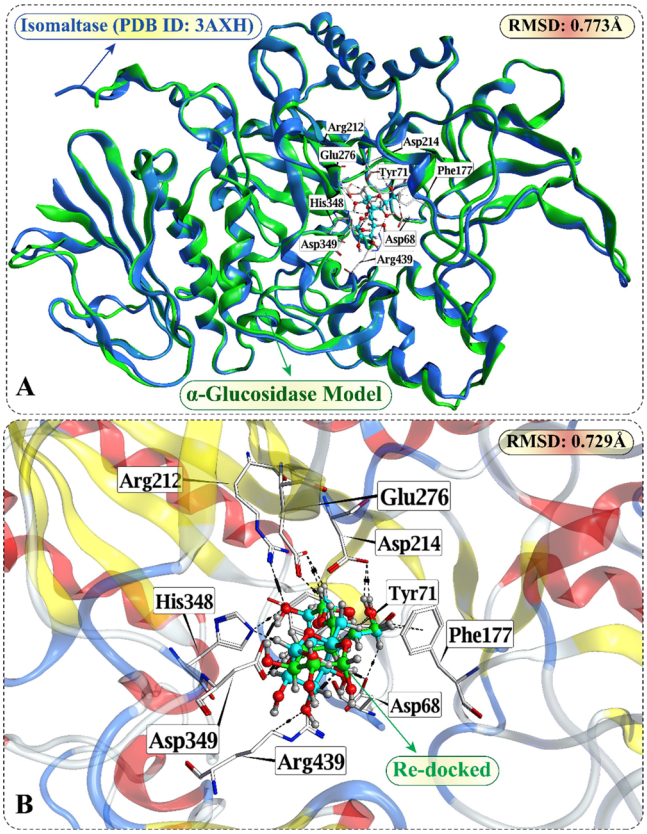

Figure 7. (A) Structural superimposition of *S. cerevisiae* isomaltase (PDB ID 3AXH) and *S. cerevisiae* a-glucosidase with the substrate molecule (isomaltose) attached in the active pocket. Protein−protein superimpose RMSD is reported. (B) Redocking of the substrate with the α-glucosidase active site residues. RMSD of the reported (cyan) and redocked (green) substrate is calculated.

The lowest docking score reported for **7l** was −4.19 kcal/mol, which had formed a single hydrogen bond with the Gly217 backbone while making two arene hydrogen interactions with Phe157 and Glu276 (Tables 2 and 3). All the compounds showed good negative interaction energies with the active pocket residues and fulfill the criteria of druglike properties. These interactions, binding energies, and affinities support the prominent α-glucosidase inhibition of the target compounds. Compounds having a good IC_{50} value from 0.64 to 20 μM include **7c**, **7f**, **7g**, **7i**, **7a**, **7e**, **7h**, **7j**, and **7m** which shows a high docking score greater than −6 kcal/mol except for **7d** for which the docking score is −5.86 kcal/mol. In contrast, the lowest IC_{50} value reported for the **7l** shows a docking score as −4.19 kcal/mol and the lowest binding energy of −29.98 kcal/mol. In the case of **7b** and **7k**, the reported docking score is −5.7 kcal/mol, whereas the IC_{50} values reported are 27.26 and 70.28 μM, respectively. The results indicate that the docking score values satisfied the in vitro inhibition assay of the α-glucosidase.

EXPERIMENTAL SECTION

Solvents and reagents of analytical grade were purchased from Daejung, Alfa Aesar, Merck, and Sigma Aldrich and were used as such. All the reactions were carried out in round-bottom flasks (Pyrex) over a hotplate magnetic stirrer and their progress was monitored by TLC analysis. Melting points were determined on Gallenkamp digital melting point equipment MGB-595-010 M. ^{1}H NMR spectra were recorded via a Bruker 600 MHz ASCEND spectrometer. Chemical shifts are given in ppm, with TMS used as an internal standard. Coupling patterns are described as s (singlet); d (doublet); t (triplet); q (quartet); and m (multiplet), and the coupling constants (J values) were reported in Hertz (Hz). ^{13}C NMR spectra were recorded via a Bruker 150 MHz ASCEND spectrometer. Chemical shifts are given in ppm, with TMS used as an internal standard. ESI-HRMS spectra were recorded on an Agilent 6530 Accurate Mass Q-TOF LC/MS system performed at the University of Nizwa, Oman.

Synthesis of Benzene-1,2-Diamine 2. 2-Nitroaniline **1** and zinc dust (0.1:0.2 mol) were taken in methanol and stirred at room temperature. Then, hydrazinium monoformate was added and stirred for 2−5 min. After completion, the reaction mixture was filtered and dried. The product was extracted in ethyl acetate, washed with brine, dried, and preserved for the next reaction.[19] Brownish solid; yield: 80%; m.p: 100−103 °C.

Synthesis of 1*H*-Benzo[*d*]imidazole-2-thiol 3. Equimolar amounts of KOH and CS_2 (0.06: 0.06 mol) were taken in ethanol−water (50:40 mL) and stirred. Then, benzene-1,2-diamine (0.06 mol) **2** was added and refluxed for 12 h. After completion, the excess solvent was removed. The product was precipitated in dilute HCl, filtered, dried, and recrystallized.[20] Off white crystals; yield: 85%; m.p: 300−303 °C.

Synthesis of 5-Nitro-1*H*-benzo[*d*]imidazole-2-thiol 4. The previous compound **3** (0.03 mol) was taken with chilling in conc. H_2SO_4 (8 mL) and a mixture of conc. HNO_3 and conc. H_2SO_4 (1:2) was added dropwise keeping overnight. Then, the reaction mixture was quenched with freezing water and the pH was made 9 by adding 10% NaOH solution. The product precipitated was filtered, washed, and dried.[21] Brownish solid; yield: 84%; m.p: 273−275 °C.

Synthesis of 5-Amino-1*H*-benzo[*d*]imidazole-2-thiol 5. Compound **5** was synthesized in a similar manner as compound **2** using Zn dust and hydrazinium monoformate.[19] Off white crystals; yield: 82%, m.p 239−242 °C.

Synthesis of 5-(Arylideneamino)-1*H*-benzo[*d*]-imidazole-2-thiols 7a−m. The target compounds **7a−m** were finally synthesized by refluxing the equimolar amounts of **5** with different aromatic aldehydes **6a−m** for 4−6 h catalyzed using 3−5 drops of organic or mineral acids.[11] After completion, the product was precipitated in freezing water, filtered, washed, and dried. All the compounds were colored solids, having high melting points and soluble in polar solvents. Their details are given below.

4-(((2-Mercapto-1*H*-benzo[*d*]imidazol-5-yl)imino)-methyl)phenol 7a. Brownish solid; yield: 87%; m.p: 245−247 °C. **^{1}H NMR** (600 MHz, DMSO): δ_H = 12.528−12.510 (s, 2H, Ar−SH, Ar−NH), 8.487 (s, 1H, Ar−N=CH), 7.768−7.755 (d, J = 7.8 Hz, 2H, Ar−H), 7.121−7.107 (d, J = 8.4 Hz, 1H, Ar−H), 7.043−7.029 (d, J = 8.4 Hz, 1H, Ar−H), 6.967 (s, 1H, Ar−H), 6.870−6.858 (d, J = 8.4 Hz, 2H, Ar−H), 4.933 (s, 1H, Ar−OH) ppm. **^{13}C NMR** (150 MHz, DMSO) δ_C = 168.48, 160.51, 159.07, 147.07, 133.06, 130.59, 130.43, 127.65, 116.62, 115.64, 109.69, 101.27 ppm. **ESI-HRMS** m/z: 270.06 $(M + H)^+$; calcd: 269.06 ($C_{14}H_{11}N_3OS$).

5-((4-Chlorobenzylidene)amino)-1*H*-benzo[*d*]-imidazole-2-thiol 7b. Light brown solid; yield: 83%; m.p: 280−282 °C. **^{1}H NMR** (600 MHz, DMSO): δ_H = 12.611−12.574 (s, 2H, Ar−SH, Ar−NH), 8.683 (s, 1H, Ar−N=CH), 7.953−7.940 (d, J = 7.8 Hz, 2H, Ar−H), 7.580−7.567 (d, J = 7.8 Hz, 2H, Ar−H), 7.158−7.119 (q, J = 8 Hz, 2H, Ar−H,),

https://doi.org/10.1021/acsomega.2c03854
ACS Omega 2022, 7, 43468−43479

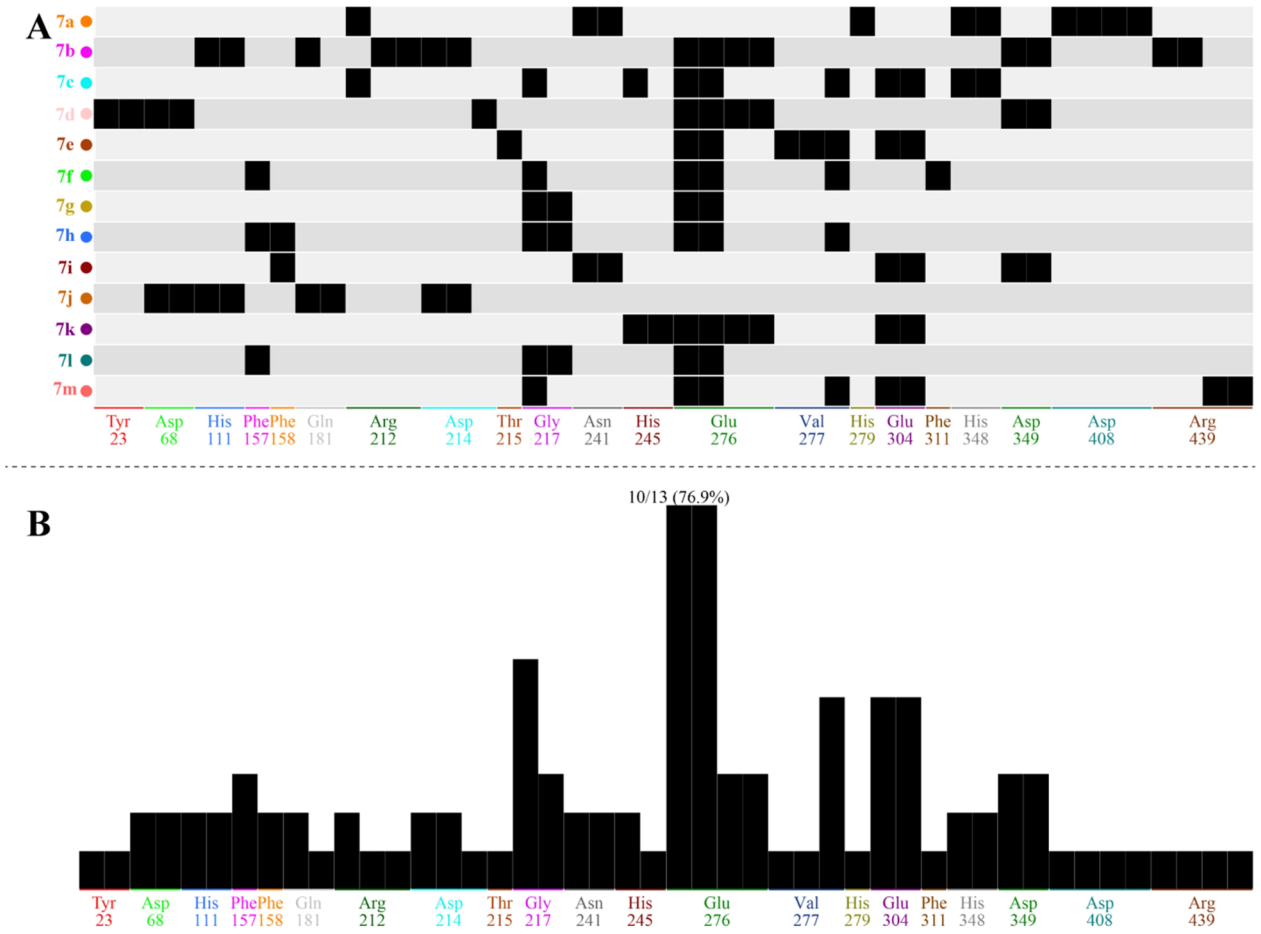

Figure 8. Docking interactions of **7a−m**. (A) Compounds interacting with the active site residues of the α-glucosidase are represented by a barcode. Each line shows a single compound interacting with each residue in a row. (B) Overall population of the interacting active pocket residues of the α-glucosidase.

7.012 (s, 1H, Ar−H) ppm. **^{13}C NMR** (150 MHz, DMSO) δ_C = 168.82, 158.26, 146.03, 135.83, 135.06, 133.07, 131.13, 130.19, 128.96, 117.05, 109.74, 101.53 ppm. **ESI-HRMS** *m*/*z*: 288.03 $(M + H)^+$; calcd: 287.03 ($C_{14}H_{10}ClN_3S$).

5-((4-Nitrobenzylidene)amino)-1*H*-benzo[*d*]-imidazole-2-thiol 7c. Red solid; yield: 87%; m.p: 283−285 °C. **^{1}H NMR** (600 MHz, DMSO): δ_H = 12.672−12.626 (s, 2H, Ar−SH, Ar−NH), 8.863 (s, 1H, Ar−N═CH), 8.353−8.339 (d, *J* = 8.4 Hz, 2H, Ar−H), 8.183−8.170 (d, *J* = 7.8 Hz, 2H, Ar−H), 7.158−7.144 (m, 3H, Ar−H) ppm. **^{13}C NMR** (150 MHz, DMSO) δ_C = 169.08, 157.41, 148.68, 145.41, 141.79, 133.10, 131.72, 129.50, 124.04, 117.58, 109.79, 101.74 ppm. **ESI-HRMS** *m*/*z*: 299.05 $(M + H)^+$; calcd: 298.05 ($C_{14}H_{10}N_4O_2S$).

5-((4-(Diethylamino)benzylidene)amino)-1*H*-benzo-[*d*]imidazole-2-thiol 7d. Deep brown solid; yield: 93%; m.p: 280−283 °C. **^{1}H NMR** (600 MHz, DMSO): δ_H = 12.496−12.479 (s, 2H, Ar−SH, Ar−NH), 8.396 (s, 1H, Ar−N═CH), 7.709−7.696 (d, *J* = 7.8 Hz, 2H, Ar−H), 7.103−7.089 (d, *J* = 8.4 Hz, 1H, Ar−H,), 7.016−7.002 (d, *J* = 8.4 Hz, 1H, Ar−H), 6.933 (s, 1H, Ar−H), 6.733−6.720 (d, *J* = 7.8 Hz, 2H, Ar−H), 3.421−3.388 (q, *J* = 7 Hz, 4H, Ar−N(CH_2)$_2$), 1.125−1.103 (t, *J* = 7 Hz, 6H, Ar−N(CH_3)$_2$) ppm. **^{13}C NMR** (150 MHz, DMSO): δ_C = 168.30, 158.92, 149.83, 133.09, 130.63, 130.07, 116.52, 110.90, 109.66, 101.09, 43.86, 12.47 ppm. **ESI-HRMS** *m*/*z*: 325.14 $(M + H)^+$; calcd: 324.14 ($C_{18}H_{20}N_4S$).

2-(((2-Mercapto-1*H*-benzo[*d*]imidazol-5-yl)imino)-methyl)-6-methoxyphenol 7e. Deep red solid; yield: 87%; m.p: 295−297 °C. **^{1}H NMR** (600 MHz, DMSO): δ_H = 12.688−12.634 (s, 2H, Ar−SH, Ar−NH), 8.965 (s, 1H, Ar−N═CH), 7.103−7.089 (d, *J* = 8.4 Hz, 1H, Ar−H), 6.899−6.873 (t, *J* = 7.8 Hz, 1H, Ar−H), 7.236−7.169 (m, 4H, Ar−H), 4.100 (s, 1H, Ar−OH), 3.805 (s, 3H, Ar−OCH_3) ppm. **^{13}C NMR** (150 MHz, DMSO): δ_C = 169.12, 162.42, 150.43, 147.89, 142.87, 133.17, 131.54, 123.90, 119.34, 118.58, 117.08, 115.39, 109.91, 101.66, 55.89 ppm. **ESI-HRMS** *m*/*z*: 300.07 $(M + H)^+$; calcd: 299.07 ($C_{15}H_{13}N_3O_2S$).

5-((2,4-Dimethoxybenzylidene)amino)-1*H*-benzo[*d*]-imidazole-2-thiol 7f. Yellowish solid; yield: 89%; m.p: 242−245 °C. **^{1}H NMR** (600 MHz, DMSO): δ_H = 12.511−12.487 (s, 2H, Ar−SH, Ar−NH), 8.736 (s, 1H, Ar−N═CH), 7.954 (s, 1H, Ar−H), 7.110−6.918 (m, 4H, Ar−H), 6.657 (s, 1H, Ar−H), 3.881−3.839 (s, 6H, Ar−OCH_3) ppm. **^{13}C NMR** (150 Hz, DMSO): δ_C = 168.48, 163.61, 160.75, 153.86, 147.53, 133.08, 130.48, 128.17, 117.18, 116.52, 109.77, 106.82, 106.56, 101.20, 98.12, 55.90, 55.58 ppm. **ESI-HRMS** *m*/*z*: 314.09 $(M + H)^+$; calcd: 313.09 ($C_{16}H_{15}N_3O_2S$).

3-Ethoxy-4-(((2-mercapto-1*H*-benzo[*d*]imidazol-5-yl)-imino)methyl)phenol 7g. Deep Brown solid; yield: 90%; m.p: 250−253 °C. **^{1}H NMR** (600 MHz, DMSO): δ_H = 12.549−12.516 (s, 2H, Ar−SH, Ar−NH), 8.470 (s, 1H, Ar−N═CH), 7.502 (s, 1H, Ar−H), 7.351−7.320 (m, 1H, Ar−H), 7.128−7.114 (d, *J* = 8.4 Hz, 1H, Ar−H), 7.055−7.041 (d, Ar−

https://doi.org/10.1021/acsomega.2c03854
ACS Omega 2022, 7, 43468−43479

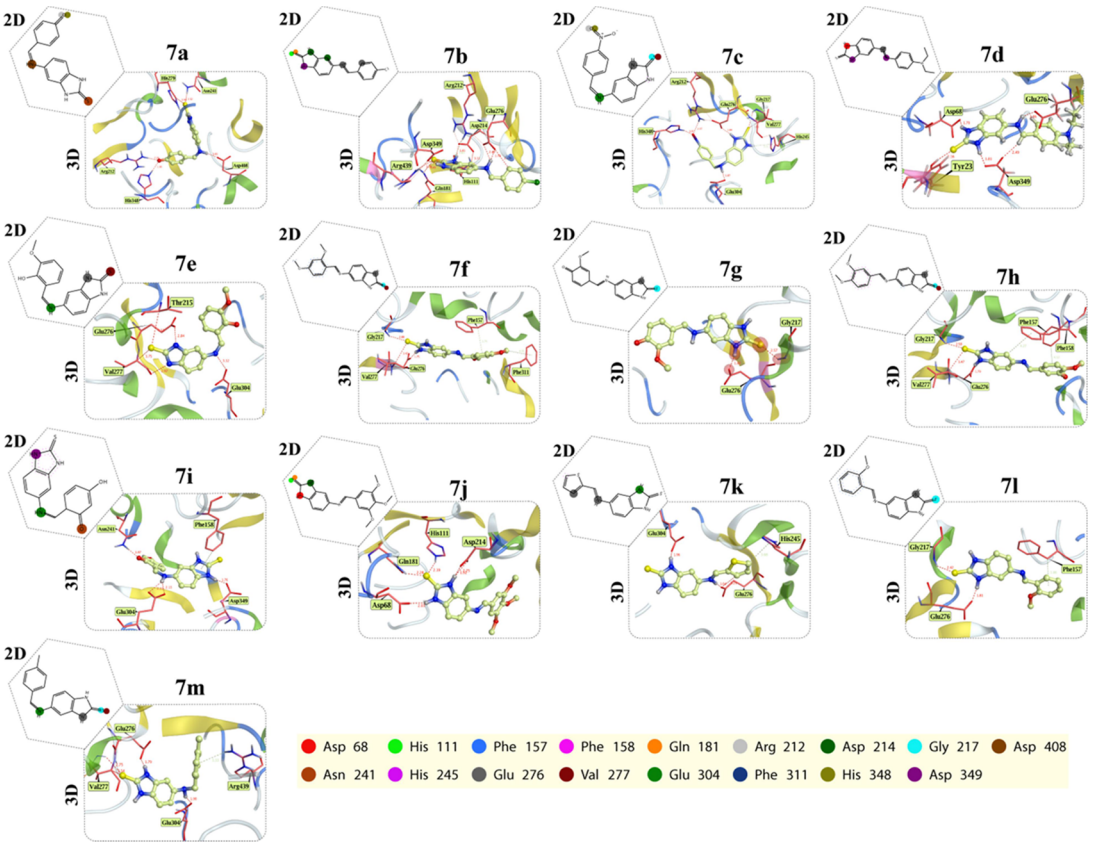

Figure 9. 2D and 3D interactions of **7a−m** in the active pocket of the α-glucosidase. Hexagon represents the 2D interaction diagram of each compound with different colored label residues while the rectangle shows the 3D interaction poses of the compounds. Interacting residues are reported in stick representation.

Table 2. Binding Energy, Affinity, and Docking Score of the Target Compounds 7a−m Calculated with the Active Pocket of the α-Glucosidase

entry	docking score (kcal/mol)	binding energy (kcal/mol)	binding affinity (kcal/mol)
7a	−5.8895102	−36.95	−6.64
7b	−5.7605391	−48.66	−8.07
7c	−6.0312943	−47.16	−7.82
7d	−5.8632793	−57.02	−9.06
7e	−6.3273244	−45.27	−7.77
7f	−6.4255824	−63.36	−10.09
7g	−6.5642915	−50.7	−8.28
7h	−6.3905635	−49.06	−8.29
7i	−6.1296835	−69.65	−10.54
7j	−7.3497996	−52.12	−9.1
7k	−5.7564335	−39.56	−6.96
7l	−4.1924725	−29.98	−4.8
7m	−6.1924725	−39.98	−7.2

H, J = 8.4 Hz, 1H,), 6.985 (s, 1H, Ar−H), 6.895−6.882 (d, J = 7.8 Hz, 1H, Ar−H,), 5.05 (s, 1H, Ar−OH), 4.080−4.070 (q, J = 6 Hz, 2H, Ar−OCH_2CH_3), 1.363−1.339 (t, J = 7 Hz, 3H, Ar−OCH_2CH_3) ppm. **^{13}C NMR** (150 MHz, DMSO): δ_C = 168.49, 166.46, 159.29, 153.23, 150.40, 147.30, 147.13, 146.83, 133.28, 133.06, 130.47, 128.73, 127.92, 125.86, 123.89, 116.60, 115.48, 111.92, 111.81, 110.94, 109.86, 109.72, 101.32, 63.86, 63.88, 14.74 ppm. **ESI-HRMS** m/z: 314.09 $(M + H)^+$; calcd: 313.09 ($C_{16}H_{15}N_3O_2S$).

5-((3,4-Dimethoxybenzylidene)amino)-1*H*-benzo[*d*]-imidazole-2-thiol 7h. Yellowish solid; yield: 92%; m.p: 257−260 °C. **^{1}H NMR** (600 MHz, DMSO): δ_H = 12.563−12.553 (s, 2H, Ar−SH, Ar−NH), 8.539 (s, 1H, Ar−N═CH), 7.545 (s, 1H, Ar−H), 7.449−7.435 (d, J = 8.4 Hz, 1H, Ar−H), 7.137−7.124 (d, J = 7.8 Hz, 1H, Ar−H), 7.080−7.066 (d, J = 8.4 Hz, 2H, Ar−H), 7.007 (s, 1H, Ar−H), 3.822 (s, 6H, Ar−OCH_3) ppm. **^{13}C NMR** (150 MHz, DMSO) δ_C = 168.9, 159.5, 152.1, 149.4, 147.1, 133.4, 131.0, 129.6, 124.2, 117.1, 111.7, 110.1, 109.8, 101.7, 56.0, 55.8 ppm. **ESI-HRMS** m/z: 314.09 $(M + H)^+$; calcd: 313.09 ($C_{16}H_{15}N_3O_2S$).

4-(((2-Mercapto-1*H*-benzo[*d*]imidazol-5-yl)Imino)-methyl)benzene-1,3-diol 7i. Brownish solid; yield: 89%; m.p: 268−271 °C. **^{1}H NMR** (600 MHz, DMSO): δ_H = 12.631−12.578 (s, 2H, Ar−SH, Ar−NH), 8.800 (s, 1H, Ar−N═CH), 7.432−7.418 (d, J = 8.4 Hz, 1H, Ar−H), 7.141−7.111 (m, 3H, Ar−H), 6.391−6.377 (d, J = 8.4 Hz, 1H, Ar−H), 6.280 (s, 1H, Ar−H), 5.00 (s, 2H, Ar−OH) ppm. **^{13}C NMR** (150 MHz, DMSO) δ_C = 168.85, 162.84, 162.28, 161.63, 143.34, 134.35, 133.17, 130.94, 116.70, 112.19, 109.89, 107.82, 102.38, 101.31 ppm. **ESI-HRMS** m/z: 286.06 $(M + H)^+$; calcd: 285.06 ($C_{14}H_{11}N_3O_2S$).

5-((3,4,5-Trimethoxybenzylidene)amino)-1*H*-benzo-[*d*]imidazole-2-thiol 7j. Yellow solid; yield: 94%. m.p: 270−273 °C. **^{1}H NMR** (600 MHz, DMSO): δ_H = 12.608−12.554 (s, 2H, Ar−SH, Ar−NH), 8.571 (s, 1H, Ar−N═CH), 7.277−7.245 (s, 2H, Ar−H), 7.149−7.136 (d, J = 7.8 Hz, 1H, Ar−H), 7.101−7.087 (d, J = 8.4 Hz, 1H, Ar−H), 7.024 (s, 1H, Ar−H), 3.845−3.723 (s, 9H, Ar−OCH_3) ppm. **^{13}C NMR** (150 MHz, DMSO) δ_C = 168.68, 159.18, 153.16, 146.39, 140.22, 133.08,

https://doi.org/10.1021/acsomega.2c03854
ACS Omega 2022, 7, 43468−43479

Table 3. Binding Interactions of the Target Compounds 7a−m with the Active Site Residues of α-Glucosidase

entry	bond type	residues	energy (kcal/mol)	distance (Å)	backbone	frequency
7a	H	Arg212	−0.50	2.92		1
	H	Asn241	−3.80	3.29		1
	H	His279	−0.70	3.99		1
	H	His348	−2.90	2.87		1
	IH	Asp408	−15.19	2.86		2
7b	H	His111	−2.70	4.06		1
	H	Gln181	−1.10	4.32		1
	A	Arg212	−1.40	4.49		1
	H	Asp214	−6.80	3.05		2
	IH	Glu276	−24.65	2.99		5
	H	Asp349	−6.20	2.86		1
	H	Arg439	−2.30	3.90		1
7c	H	Arg212	−0.60	3.13		1
	H	Gly217	−1.00	3.32	b-	1
	A	His245	−0.50	4.09		1
	H	Glu276	−6.20	2.87		1
	H	Val277	−0.50	3.85	b-	1
	H	Glu304	−2.60	2.88		1
	H	His348	−3.30	2.86		1
7d	H	Tyr23	−3.30	3.10		1
	H	Asp68	−3.10	2.74		1
	IH	Glu276	−16.66	2.96		3
	H	Asp349	−3.40	3.12		2
7e	H	Thr215	−0.70	4.13	b-	1
	H	Glu276	−5.20	2.84		1
	H	Val277	−2.60	3.36	b-	2
	H	Glu304	−2.50	3.12		1
7f	A	Phe157	−0.80	3.74		1
	H	Gly217	−0.90	3.50	b-	1
	H	Glu276	−6.70	2.78		1
	H	Val277	−0.90	3.42	b-	1
	A	Phe311	−0.60	4.09		1
7g	H	Gly217	−1.70	3.27	b-	1
	H	Glu276	−6.40	2.85		1
7h	A	Phe157	−0.80	4.27		1
	A	Phe158	−0.60	4.52		1
	H	Gly217	−2.20	3.31	b-	1
	H	Glu276	−6.00	2.78		1
	H	Val277	−0.90	3.47	b-	1
7i	A	Phe158	−0.50	3.82		1
	H	Asn241	−5.20	2.87		1
	H	Glu304	−8.40	3.02		2
	H	Asp349	−6.10	2.77		1
7j	H	Asp68	−5.20	2.97		1
	H	His111	−4.00	3.13		1
	H	Gln181	−3.70	3.20		1
	H	Asp214	−7.70	3.02		2
7k	A	His245	−1.90	3.68		1
	IH	Glu276	−23.06	2.87		3
	H	Glu304	−4.30	2.83		1
	A	His245	−1.90	3.68		1
7l	A	Phe157	−0.70	3.88		1
	H	Gly217	−3.20	3.26	b-	1
	H	Glu276	−6.70	2.85		1
7m	H	Gly217	−1.20	3.40	b-	1
	H	Glu276	−6.30	2.80		1
	H	Val277	−0.70	3.54	b-	1
	H	Glu304	−2.80	2.89		1
	A	Arg439	−1.00	4.09		1

131.69, 130.84, 116.87, 109.76, 106.77, 105.81, 101.33, 60.20, 55.97 ppm. **ESI-HRMS** *m*/*z*: 344.10 $(M + H)^+$; calcd: 343.10 ($C_{17}H_{17}N_3O_3S$).

5-((Thiophen-2-ylmethylene)amino)-1*H*-benzo[*d*]-imidazole-2-thiol 7k. Yellowish solid; yield: 82%. m.p: > 300 °C. **^{1}H NMR** (600 MHz, DMSO): δ_H = 12.590−12.550 (s, 2H, Ar−SH, Ar−NH), 8.816 (s, 1H, Ar−N═CH), 7.781−7.773 (d, *J* = 4.8 Hz, 1H, Ar−H), 7.668 (s, 1H, Ar−H), 7.025−7.028 (m, 4H, Ar−H) ppm. **^{13}C NMR** (101 MHz, DMSO) δ_C = 168.73, 152.82, 145.82, 142.67, 133.36, 133.08, 130.94, 130.88, 128.26, 116.97, 109.75, 101.40 ppm. **ESI-HRMS** *m*/*z*: 260.03 $(M + H)^+$; calcd: 259.02 ($C_{12}H_9N_3S_2$).

5-((2-Methoxybenzylidene)amino)-1*H*-benzo[*d*]-imidazole-2-thiol 7l. Yellowish solid; yield: 90%; m.p: 234−237 °C. **^{1}H NMR** (600 MHz, DMSO): δ_H = 12.548−12.522 (s, 2H, Ar−SH, Ar−NH), 8.864 (s, 1H, Ar−N═CH), 8.010−7.998 (d, *J* = 7.2 Hz, 1H, Ar−H), 7.502−7.490 (t, *J* = 7.2 Hz, 1H, Ar−H), 7.158−7.130 (t, *J* = 8.4 Hz, 2H, Ar−H), 7.063−7.049 (d, *J* = 8.4 Hz, 2H, Ar−H), 6.972 (s, 1H, Ar−H), 3.887 (s, 3H, Ar−OCH_3) ppm. **^{13}C NMR** (150 MHz, DMSO) δ_C = 168.66, 159.21, 154.39, 147.09, 136.51, 133.08, 133.05, 130.85, 127.77, 126.74, 123.95, 120.71, 120.66, 116.63, 112.75, 112.04, 109.81, 101.38, 55.82 ppm. **ESI-HRMS** *m*/*z*: 284.08 $(M + H)^+$; calcd: 283.08 ($C_{15}H_{13}N_3OS$).

5-((4-Methylbenzylidene)amino)-1*H*-benzo[*d*]-imidazole-2-thiol 7m. Off white solid; yield: 88%; m.p: > 300 °C. **^{1}H NMR** (600 MHz, DMSO): δ_H = 12.559 (s, 2H, Ar−SH, Ar−NH), 8.609 (s, 1H, Ar−N═CH), 7.827−7.815 (d, *J* = 7.2 Hz, 2H, Ar−H), 7.321−7.308 (d, *J* = 7.8 Hz, 2H, Ar−H), 7.142−7.128 (d, *J* = 8.4 Hz, 1H, Ar−H), 7.098−7.085 (d, *J* = 7.8 Hz, 1H, Ar−H), 7.025 (s, 1H, Ar−H), 2.490−2.368 (s, 3H, Ar−CH_3) ppm. **^{13}C NMR** (150 MHz, DMSO) δ_C = 168.65, 159.39, 146.58, 141.32, 133.67, 133.05, 129.43, 128.62, 116.80, 109.71, 101.42, 21.20 ppm. **ESI-HRMS** *m*/*z*: 268.09 $(M + H)^+$; calcd: 267.08 ($C_{15}H_{13}N_3S$).

α-Glucosidase Inhibition Assay. The α-glucosidase inhibition potential of the target compounds **7a−m** was evaluated with reference to **acarbose.**[12] The enzyme (0.2 U/mL) taken in phosphate buffer (50 mM, pH. 6.8) was incubated with various concentrations of the compounds at 37 °C for 15 min. Then, *p*-nitrophenyl-α-D-glucopyranoside (0.7 mM) was added as the substrate. The change in absorbance at 400 nm was monitored up to 30 min by a multiplate spectrophotometer, and then, the compound was replaced by DMSO (7.5% final) as the control. All the reactions were performed in triplicate and the percent inhibition was calculated by the following formula:

$$\% \text{ Inhibition} = 100 \text{ (OD test well / OD control)} \times 100$$

Molecular Docking Simulations. The molecular docking technique was used to explore the atomic-level attachment and ligand fitting of the selected compounds with the α-glucosidase active site. MOE was used to run docking simulations on the target compounds **7a−m**. Fast Fourier Transform (FFT) was used to produce their poses near the active site. Using eq 1, the

https://doi.org/10.1021/acsomega.2c03854
ACS Omega 2022, 7, 43468−43479

R-Field electrostatics of the London dG solvation model was chosen for the revised top 30 poses.

$$\Delta G = c + E_{\text{flex}} + \sum_{\text{h-bonds}} c_{\text{HB}} f_{\text{HB}} + \sum_{\text{m-lig}} c_{\text{M}} f_{\text{M}} + \sum_{\text{atom } i} \Delta D_i \quad (1)$$

In eq 1, "*c*" calculates the gain or loss in entropy (rotational/transitional), E_{flex} determines the loss of energy in the ligand, and f_{HB} calculates the defects in the hydrogen bonds. In contrast, C_{HB} calculates the favorable hydrogen bond energy, whereas f_{M} calculates the metal ligand imperfection and C_{M} determines the ideal metal-binding energy, whereas D_i estimates the dissolution energy of each atom. The top 30 postures obtained from the London dG algorithm were improved to pick the final pose using the GBVI/WSA dG solvation technique implemented in MOE's Dock.

$$\Delta G \approx c + a\left[\frac{2}{3}(\Delta E_{\text{coul}} + \Delta E_{\text{sol}}) + \Delta E_{\text{vdw}} + \beta \Delta \text{SA}_{\text{weighted}}\right]\# \quad (2)$$

In eq 2, the increase or decrease in entropy (rotational/transitional), that is, "*c*" and "*a*" are constants that depend on the force field chosen, E_{coul} calculates Coulomb electrostatics, E_{sol} calculates solvation energies, E_{vdw} calculates the van der Waals contributions of the systems, and $\text{SA}_{\text{weighted}}$ calculates the exposed surface area. As the crystal structure of the *Saccharomyces cerevisiae*, α-glucosidase is not present. The *S. cerevisiae* isomaltase (PDB ID: 3AXH)[22] and *S. cerevisiae* α-glucosidase catalytic residues are conserved. The substrate molecule (isomaltose) cocrystallized in the isomaltase 3D structure was manually docked in the a-glucosidase by aligning the protein sequence and structure, and the RMSD of the protein structure and sequence alignment was reported.[23] To validate the docking protocols, the redocking was performed using the substrate molecule with the α-glucosidase active site residues. The superimposed RMSD of the reported substrate and the redocked substrate was calculated in angstrom (Å). The 2D structures of the target compounds **7a**−**m** were drawn using ChemDraw, transformed to 3D, and saved in the MOE database.[24] The compounds were washed and the energy was reduced using the MMFF94X force field. Then, docking techniques were used to molecularly attach these compounds with the active pocket of the α-glucosidase. The final refine pose for each compound was saved in the MDB format with the energies calculated in the database.

CONCLUSIONS

A series of 13 novel benzimidazoles **7a**−**m** was synthesized, characterized via MS and NMR techniques, and assessed for their in vitro α-glucosidase inhibitory potential. All the compounds showed prominent inhibition of the enzyme (IC_{50} range: 0.64 ± 0.05 μM to 343.10 ± 1.62 μM) as compared to **acarbose** (IC_{50}: 873.34 ± 1.21) where **7i** showed the highest activity (IC_{50}: 0.64 ± 0.05 μM). Molecular docking further supported the effective enzyme inhibition of these compounds in terms of the docking score, binding energy, and affinity. These promising results could be utilized in drug development against type 2 diabetes mellitus.

ASSOCIATED CONTENT

Supporting Information

The Supporting Information is available free of charge at https://pubs.acs.org/doi/10.1021/acsomega.2c03854.

Details of the spectroscopic data including ESI-HRMS, ^{1}HNMR, and ^{13}CNMR (PDF)

AUTHOR INFORMATION

Corresponding Authors

Sardar Ali − *Department of Chemistry, University of Malakand, Chakdara 18800 Khyber Pakhtunkhwa, Pakistan;* orcid.org/0000-0001-6514-4003; Email: sardaraliiuom@gmail.com

Mumtaz Ali − *Department of Chemistry, University of Malakand, Chakdara 18800 Khyber Pakhtunkhwa, Pakistan;* orcid.org/0000-0001-7573-7953; Email: mumtazphd@gmail.com

Authors

Ajmal Khan − *Natural and Medical Sciences Research Center, University of Nizwa, Nizwa 616, Oman*

Saeed Ullah − *Natural and Medical Sciences Research Center, University of Nizwa, Nizwa 616, Oman; H. E. J Research Institute of Chemistry, International Center for Chemical and Biological Sciences, University of Karachi, Karachi 75270, Pakistan*

Muhammad Waqas − *Natural and Medical Sciences Research Center, University of Nizwa, Nizwa 616, Oman; Department of Biotechnology and Genetic Engineering, Hazara University, Mansehra 21120, Pakistan*

Ahmed Al-Harrasi − *Natural and Medical Sciences Research Center, University of Nizwa, Nizwa 616, Oman;* orcid.org/0000-0002-0815-5942

Abdul Latif − *Department of Chemistry, University of Malakand, Chakdara 18800 Khyber Pakhtunkhwa, Pakistan*

Manzoor Ahmad − *Department of Chemistry, University of Malakand, Chakdara 18800 Khyber Pakhtunkhwa, Pakistan;* orcid.org/0000-0001-9736-5900

Muhammad Saadiq − *Department of Chemistry, Bacha Khan University, Charsadda 18800 Khyber Pakhtunkhwa, Pakistan;* orcid.org/0000-0002-4963-4341

Complete contact information is available at: https://pubs.acs.org/10.1021/acsomega.2c03854

Notes

The authors declare no competing financial interest.

ACKNOWLEDGMENTS

This work was funded by the Higher Education Commission of Pakistan (HEC) under National Research Project for University (NRPU), No: 20-2892, which is titled as "*Synthesis and characterization of benzimidazole derivatives with potential pharmacological significance*".

REFERENCES

(1) (a) Flefel, E. M.; El-Sofany, W. I.; Al-Harbi, R. A.; El-Shahat, M. Development of a novel series of anticancer and antidiabetic: spirothiazolidines analogs. *Molecules* **2019**, *24*, 2511. (b) Kajaria, D.; Ranjana, J. T.; Tripathi, Y. B.; Tiwari, S. In-vitro α amylase and glycosidase inhibitory effect of ethanolic extract of antiasthmatic drug—Shirishadi. *J. Adv. Pharm. Technol. Res.* **2013**, *4*, 206.

(2) (a) Dayma, V.; Chopra, J.; Sharma, P.; Dwivedi, A.; Tripathi, I. P.; Bhargava, A.; Murugesan, V.; Goswami, A. K.; Baroliya, P. K. Synthesis, antidiabetic, antioxidant and anti-inflammatory activities of novel hydroxytriazenes based on sulpha drugs. *Heliyon* **2020**, *6*, No. e04787. (b) Poovitha, S.; Parani, M. In vitro and in vivo α-amylase and α-glucosidase inhibiting activities of the protein extracts from two varieties of bitter gourd (Momordica charantia L.). *BMC Complementary Altern. Med.* **2016**, *16*, 185.
(3) Keri, R. S.; Patil, M. R.; Patil, S. A.; Budagumpi, S. A comprehensive review in current developments of benzothiazole-based molecules in medicinal chemistry. *Eur. J. Med. Chem.* **2015**, *89*, 207−251.
(4) Wagman, A. S.; Boyce, R. S.; Brown, S. P.; Fang, E.; Goff, D.; Jansen, J. M.; Le, V. P.; Levine, B. H.; Ng, S. C.; Ni, Z.-J. Synthesis, binding mode, and antihyperglycemic activity of potent and selective (5-imidazol-2-yl-4-phenylpyrimidin-2-yl)[2-(2-pyridylamino) ethyl] amine inhibitors of glycogen synthase kinase 3. *J. Med. Chem.* **2017**, *60*, 8482−8514.
(5) (a) Tundis, R.; Loizzo, M.; Menichini, F. Natural products as α-amylase and α-glucosidase inhibitors and their hypoglycaemic potential in the treatment of diabetes: an update. *Mini-Rev. Med. Chem.* **2010**, *10*, 315−331. (b) Sansenya, S.; Winyakul, C.; Nanok, K.; Phutdhawong, W. S. Synthesis and inhibitory activity of N-acetylpyrrolidine derivatives on α-glucosidase and α-amylase. *Res. Pharm. Sci.* **2020**, *15*, 14. (c) Gong, L.; Feng, D.; Wang, T.; Ren, Y.; Liu, Y.; Wang, J. Inhibitors of α-amylase and α-glucosidase: Potential linkage for whole cereal foods on prevention of hyperglycemia. *Food Sci. Nutr.* **2020**, *8*, 6320−6337.
(6) Aamir, A. H.; Ul-Haq, Z.; Mahar, S. A.; Qureshi, F. M.; Ahmad, I.; Jawa, A.; Sheikh, A.; Raza, A.; Fazid, S.; Jadoon, Z.; Ishtiaq, O.; Safdar, N.; Afridi, H.; Heald, A. H. Diabetes Prevalence Survey of Pakistan (DPS-PAK): prevalence of type 2 diabetes mellitus and prediabetes using HbA1c: a population-based survey from Pakistan. *BMJ Open* **2019**, *9*, No. e025300.
(7) Adnan, M.; Aasim, M. Prevalence of type 2 diabetes mellitus in adult population of Pakistan: A meta-analysis of prospective cross-sectional surveys. *Ann. Global Health* **2020**, *86*, 7.
(8) Federation, I. D. *IDF DIABETES ATLAS Ninth edition 2019*, 2019.
(9) (a) Akhtar, W.; Khan, M. F.; Verma, G.; Shaquiquzzaman, M.; Rizvi, M.; Mehdi, S. H.; Akhter, M.; Alam, M. M. Therapeutic evolution of benzimidazole derivatives in the last quinquennial period. *Eur. J. Med. Chem.* **2017**, *126*, 705−753. (b) Kalinina, T.; Shimshirt, A.; Volkova, A.; Korolev, A.; Voronina, T. Anxiolytic Effects of Diazepam and Afobazole on the Anxiety Response Evoked by GABA (A) Receptor Blockade in Wistar Rats and Inbred Mice of Balb/c And C57BI/6 Strains. *Eksp. Klin. Farmakol.* **2016**, *79*, 3−7. (c) Bischof, J.; Leban, J.; Zaja, M.; Grothey, A.; Radunsky, B.; Othersen, O.; Strobl, S.; Vitt, D.; Knippschild, U. 2-Benzamido-N-(1 H-benzo [d] imidazol-2-yl) thiazole-4-carboxamide derivatives as potent inhibitors of CK1δ/ε. *Amino Acids* **2012**, *43*, 1577−1591. (d) Subramanian, S.; Costales, A.; Williams, T. E.; Levine, B.; McBride, C. M.; Poon, D.; Amiri, P.; Renhowe, P. A.; Shafer, C. M.; Stuart, D.; Verhagen, J.; Ramurthy, S. Design and synthesis of orally bioavailable benzimidazole reverse amides as pan RAF kinase inhibitors. *ACS Med. Chem. Lett.* **2014**, *5*, 989−992.
(10) (a) Yadav, S.; Narasimhan, B.; Lim, S. M.; Ramasamy, K.; Vasudevan, M.; Shah, S. A. A.; Selvaraj, M. Synthesis, characterization, biological evaluation and molecular docking studies of 2-(1H-benzo [d] imidazol-2-ylthio)-N-(substituted 4-oxothiazolidin-3-yl) acetamides. *Chem. Cent. J.* **2017**, *11*, 137. (b) Mavrova, A. T.; Anichina, K. K.; Vuchev, D. I.; Tsenov, J. A.; Denkova, P. S.; Kondeva, M. S.; Micheva, M. K. Antihelminthic activity of some newly synthesized 5 (6)-(un) substituted-1H-benzimidazol-2-ylthioacetylpiperazine derivatives. *Eur. J. Med. Chem.* **2006**, *41*, 1412−1420. (c) Shingalapur, R. V.; Hosamani, K. M.; Keri, R. S. Synthesis and evaluation of in vitro anti-microbial and anti-tubercular activity of 2-styryl benzimidazoles. *Eur. J. Med. Chem.* **2009**, *44*, 4244−4248. (d) Demirayak, Ş.; Yurttaş, L. Synthesis and anticancer activity of some 1, 2, 3-trisubstituted pyrazinobenzimidazole derivatives. *J. Enzyme Inhib. Med. Chem.* **2014**, *29*, 811−822. (e) Kamil, A.; Akhtar, S.; Jahan, S.; Karim, A.; Rafiq, K.; Hassan, S. Benzimidazole derivatives: active class of antioxidants. *J. Sci. Eng. Res.* **2013**, *4*, 1674−1685. (f) Latif, A.; Bibi, S.; Ali, S.; Ammara, A.; Ahmad, M.; Khan, A.; Al-Harrasi, A.; Ullah, F.; Ali, M. New multitarget directed benzimidazole-2-thiol-based heterocycles as prospective anti-radical and anti-Alzheimer's agents. *Drug Dev. Res.* **2021**, *82*, 207−216.
(11) (a) Ali, M.; Ali, S.; Khan, M.; Rashid, U.; Ahmad, M.; Khan, A.; Al-Harrasi, A.; Ullah, F.; Latif, A. Synthesis, biological activities, and molecular docking studies of 2-mercaptobenzimidazole based derivatives. *Bioorg. Chem.* **2018**, *80*, 472−479. (b) Saadiq, M.; Uddin, G.; Latif, A.; Ali, M.; Akbar, N.; Ammara; Ali, S.; Ahmad, M.; Zahoor, M.; Khan, A.; et al. Synthesis, Bioactivity Assessment, and Molecular Docking of Non-sulfonamide Benzimidazole-Derived N-Acylhydrazone Scaffolds as Carbonic Anhydrase-II Inhibitors. *ACS Omega* **2022**, *7*, 705−715.
(12) Kashtoh, H.; Hussain, S.; Khan, A.; Saad, S. M.; Khan, J. A.; Khan, K. M.; Perveen, S.; Choudhary, M. I. Oxadiazoles and thiadiazoles: novel α-glucosidase inhibitors. *Bioorg. Med. Chem.* **2014**, *22*, 5454−5465.
(13) Jumper, J.; Evans, R.; Pritzel, A.; Green, T.; Figurnov, M.; Ronneberger, O.; Tunyasuvunakool, K.; Bates, R.; Žídek, A.; Potapenko, A.; Bridgland, A.; Meyer, C.; Kohl, S. A. A.; Ballard, A. J.; Cowie, A.; Romera-Paredes, B.; Nikolov, S.; Jain, R.; Adler, J.; Back, T.; Petersen, S.; Reiman, D.; Clancy, E.; Zielinski, M.; Steinegger, M.; Pacholska, M.; Berghammer, T.; Bodenstein, S.; Silver, D.; Vinyals, O.; Senior, A. W.; Kavukcuoglu, K.; Kohli, P.; Hassabis, D. Highly accurate protein structure prediction with AlphaFold. *Nature* **2021**, *596*, 583−589.
(14) Anderson, R. J.; Weng, Z.; Campbell, R. K.; Jiang, X. Main-chain conformational tendencies of amino acids. *Proteins: Struct., Funct., Bioinf.* **2005**, *60*, 679−689.
(15) Wiederstein, M.; Sippl, M. J. ProSA-web: interactive web service for the recognition of errors in three-dimensional structures of proteins. *Nucleic Acids Res.* **2007**, *35*, W407−W410.
(16) ULC, C. C. G. *Molecular Operating Environment (MOE)*, 2020.09. 2020.
(17) Allaire, G.; Dapogny, C.; Frey, P. A mesh evolution algorithm based on the level set method for geometry and topology optimization. *Struct. Multidiscip. Optim.* **2013**, *48*, 711−715.
(18) Yamamoto, K.; Miyake, H.; Kusunoki, M.; Osaki, S. Crystal structures of isomaltase from Saccharomyces cerevisiae and in complex with its competitive inhibitor maltose. *FEBS J.* **2010**, *277*, 4205−4214.
(19) Gowda, S.; Kempe Gowda, B.; Channe Gowda, D. Hydrazinium monoformate: A new hydrogen donor. Selective reduction of nitrocompounds catalyzed by commercial zinc dust. *Synth. Commun.* **2003**, *33*, 281−289.
(20) Rizvi, S. F. A.; Zhang, H.; Mehmood, S.; Sanad, M. Synthesis of 99mTc-labeled 2-Mercaptobenzimidazole as a novel radiotracer to diagnose tumor hypoxia. *Transl. Oncol.* **2020**, *13*, No. 100854.
(21) Zurabishvili, D. S.; Bukia, T. J.; Lomidze, M. O.; Trapaidze, M. V.; Elizbarashvili, E. N.; Samsoniya, S. A.; Doroshenko, T. V.; Kazmaier, U. Preparation of 2-(1-adamantyl)-1 H-benzimidazole and novel derivatives thereof. *Chem. Heterocycl. Compd.* **2015**, *51*, 139−145.
(22) Yamamoto, K.; Miyake, H.; Kusunoki, M.; Osaki, S. Steric hindrance by 2 amino acid residues determines the substrate specificity of isomaltase from Saccharomyces cerevisiae. *J. Biosci. Bioeng.* **2011**, *112*, 545−550.
(23) Halim, S. A.; Jabeen, S.; Khan, A.; Al-Harrasi, A. Rational Design of Novel Inhibitors of α-Glucosidase: An Application of Quantitative Structure Activity Relationship and Structure-Based Virtual Screening. *Pharmaceuticals* **2021**, *14*, 482.
(24) Mills, N. ChemDraw Ultra 10.0 CambridgeSoft, 100 CambridgePark Drive, Cambridge, MA 02140. www. cambridgesoft. com. Commercial Price: 1910fordownload, 2150 for CD-ROM;

https://doi.org/10.1021/acsomega.2c03854
ACS Omega 2022, 7, 43468−43479

Academic Price: 710fordownload, 800 for CD-ROM. ACS Publications, 2006.

https://doi.org/10.1021/acsomega.2c03854
ACS Omega 2022, 7, 43468−43479